COLD MAGNETOSPHERIC PLASMA FLOWS AND SPACECRAFT WAKES: PICUP3D SIMULATIONS AND CLUSTER DATA

E. Engwall (Erik.Engwall@irfu.se)[1,2] and A. I. Eriksson (Anders.Eriksson@irfu.se)[2]

[1] *Department of Astronomy and Space Physics, Uppsala University, Sweden*
[2] *Swedish Institute of Space Physics, Uppsala, Sweden*
Tel: +46 18 471 59 00
Fax: +46 18 471 59 05

Behind a spacecraft in a supersonic ion flow, a negatively charged wake will form. In a sufficiently tenuous plasma, where the potential of a sunlit spacecraft becomes positive, the size of the ion wake can become very much larger than what may be expected from the spacecraft geometrical size. This occurs if the energy of the flowing ions is less than what is needed to overcome the positive spacecraft potential. As the ion flow must be supersonic, this means that the plasma flow has to be quite cold. It turns out that such conditions are quite common in the terrestrial magnetosphere, particularly in the polar wind region. The polar wind cold plasma flow at geocentric distances outside 10 Earth radii can have ion flow kinetic energy around 10 eV, ion temperature of a few eV and be so tenuous that the potential of a spacecraft reaches above 20 V. This plasma is rarely measured on scientific spacecraft, as the ions cannot reach an ion detector mounted on the highly positive spacecraft. Consequently, there are only a few studies of its properties and distribution. However, the cold ion density can be estimated by comparing the number of ions actually detected on the spacecraft with independent density estimates, for example spacecraft potential measurements or wave signatures. Another effect of the negatively charged wake is its impact on electric field measurements on the spacecraft, which shows a clear signature of the wake electrostatic potential. While this is a contamination to the measurement of the natural electric field, it is also potentially useful to derive flow properties like velocity and temperature. In order to understand the problems and exploit the possibilities of this effect, we have analyzed data from the Cluster double probe instrument EFW and used the PicUp3D code to perform PIC simulations. This study has given new information on the properties of the wake, as well as the photoemission from the electric field probes.

1. Introduction

Cold ions with temperatures of a few eV are common in the magnetosphere. However, they are difficult to measure with conventional ion instruments, since the spacecraft potential of a sunlit spacecraft in a tenuous plasma often is of the order of several tens of volts, preventing the cold ions from reaching the spacecraft. Recent studies have been able to detect cold ions for high ion drift velocities or with spacecraft equipped with artificial spacecraft potential control. Su et al [1] have been able to measure the properties of the cold flowing polar wind with the POLAR spacecraft, equipped with the ion instrument TIDE and the artificial plasma source instrument PSI, which brings the spacecraft potential as low as 1 V. Sauvaud et al. have performed measurements with the ion spectrometer CIS onboard Cluster, which detected cold ions accelerated by an intermittently moving magnetopause [2] and fast flowing cold ions in the magnetotail [3].

Cold flowing plasmas form a wake behind the spacecraft. Signatures of this wake can be seen in the data from a double-probe electric field instrument like the EFW instrument on Cluster. The wake signature is mostly seen as a contamination of the real electric field which the instrument aims at observing, but if properly understood, the wake signature holds a potential for deriving properties of the cold flowing plasma. We have therefore analyzed data from EFW and performed simulations of the wake formation using the code package PicUp3D [4]. Simulations constitute an important complement to data analysis, since the dependence of the wake properties on plasma parameters such as ion temperature are difficult to measure, as the cold ions are difficult to detect with ion spectrometers. The data analysis has, in addition to better understanding of the wake, given new information on the assymmetric photoemission from the double probes, causing a sunward spurious electric field.

The paper starts with some general remarks on the wake in EFW data, followed by a section on simulations of the wake formation. The results from the simulations complement the double-probe data analysis presented in section 3. In sections 4 and 5, Discussion and Conclusions can be found.
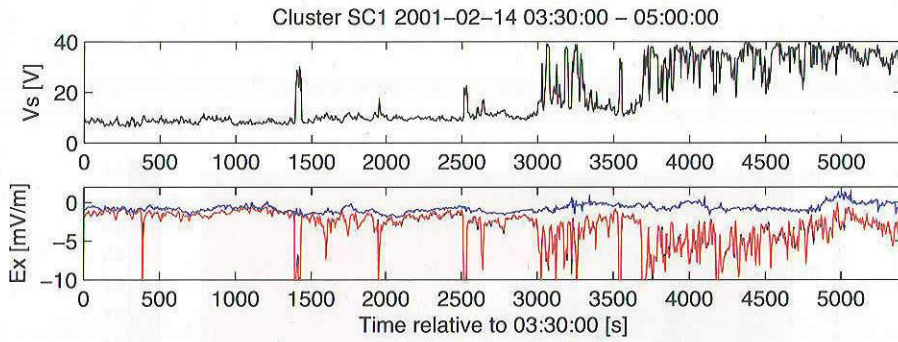
Fig. 1. EFW and EDI electric field data from Cluster 1. The top panel shows the spacecraft potential V_s, while the lower panel displays the EDI (blue) and EFW (red, black) estimates of the GSE X component of the electric field. Strong discrepancies between the EDI and EFW electric field estimates can be seen when V_s is high. (After Engwall et al. [9].)

2. Evidence of spacecraft wake in Cluster data

The Cluster satellites are equipped with two instruments for electric field measurements using different techniques: the Electric Fields and Waves instrument (EFW) [5] and the Electron Drift Instrument (EDI) [6]. EFW uses the well-known and conceptually simple technique of two spherical probes measuring the potential difference in the plasma. The probes are separated by 88 m thin wire booms spinning in a plane very close to the ecliptical plane (GSE X-Y- plane). EDI measures the electric field by determining the drift of high-energetic electrons in a magnetized plasma. Both techniques have their own weaknesses and merits [7]. When operating in cold flowing plasmas, a direct interpretation of EFW data gives an electric field estimate differing from what is observed by EDI. An example from the polar wind is shown in Figure 1. In this Figure it can also clearly be seen that the problems grow when the spacecraft potential is high.

The explanation to the spurious electric field is that an enhanced wake is formed behind the spacecraft [7]. This wake will be much larger than expected from the geometrical size of the spacecraft, if the spacecraft potential is larger than the supersonic flow energy of the ions, i.e. if the following inequality is satisfied

$$KT_i < E_k^i < eV_s, \tag{1}$$

where KT_i and V_s are the ion thermal energy and the spacecraft potential, respectively. For such conditions, the ions will be deflected by the potential structures rather than the geometrical shape of the spacecraft. In addition, not only the spacecraft body will contribute to the wake, but also the thin wire booms, since their effective size will grow from a few millimeters to the order of meters.

3. Simulations of the wake

To study the wake formation behind Cluster and the effect on EFW, we have performed simulations with PicUp3D. The simulations may also provide some information on the dependence of the wake properties on plasma parameters such as ion temperature, which is useful since the cold ions are difficult to measure *in situ* with conventional ion detectors. We have run two types of simulations for typical polar wind conditions [1]: The wake effect behind a) one pair of the wire booms only, and b) the spacecraft body only. This division is made to simplify the simulations, but also to better understand the contributions to the wake from different parts of the spacecraft system. The simulations with the booms have indeed shown that they can by themselves create a wake giving rise to a spurious electric field of over 5 mV/m, assuming the probes perfectly couple to the plasma [8] [9]. This is comparable to the spurious electric field in EFW data of 5-10 mV/m.

In Figure 2 the ion density from one of the simulations with the spacecraft only is displayed, showing a clear depletion behind the spacecraft. This ion wake will to a large extent be filled with the subsonic electrons creating a negatively charged wake behind the spacecraft. This can be seen in Figure 3, where the potential contours around the spacecraft are shown. The effect on the double-probe instrument mounted on a spinning spacecraft for different plasma parameters is shown in Figure 4, which indeed show the same overall shape as EFW data. From the simulations, it is evident that size of the wake, as well as the signatures are dependent on the plasma parameters. Thus, by careful examination of the signatures of the spurious EFW signal in combination with the simulation results, there is a potential to derive properties of the flowing plasma. By another method, it is possible to calculate the flow velocity only from comparison between EFW and EDI data, provided that certain conditions apply and that we know the angle of the flowing plasma in the spin

---

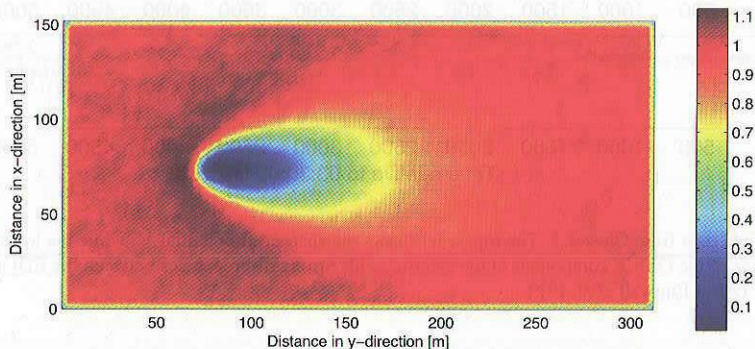[1] E_k^i=10 eV, KT_i=1-2 eV, KT_e=1-2 eV, n_0=0.2 cm^{-3}, V_s=35 V.

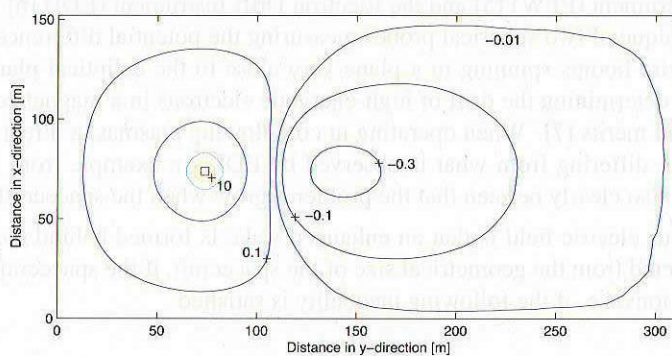Fig. 2. Ion density around the spacecraft, which is situated at x=78 m and y=78 m.

Fig. 3. Potential contours around the spacecraft, the potential of which is 35 V. The minimum potential in the wake is -0.34 mV.

plane, which we can find using the method described in section 4.2. From the sounding experiment WHISPER on Cluster as well as from measurements of the spacecraft potential, the plasma density can be estimated. The remaining two free parameters, the electron and ion temperatures, could possibly be obtained by careful examination of the signatures of the spurious EFW signal in comparison with the simulation results.

4. Analysis of double-probe data

4.1 Sunward offset field

Since the Cluster spacecraft are spinning, the voltage difference between two oppositely mounted probes varies sinusoidally in time if there is a constant and homogeneous electric field and the instrument is ideal. At first, we study the signal always present in double-probe measurements [10], because of asymmetric photoemission. This appears as a spurious sunward directed electric field signal ($E_X^{\mathrm{GSE}} > 0$; see panel (b) of Figure 6.1), though it is not due to any macroscopic E-field, only to the inevitably imperfect illumination symmetry of the instrument.

To study the effect, we choose an interval where EDI and EFW agrees on GSE E_y, and the E_x component is small in EDI data. By Fourier analysis of the double-probe signal together with EDI data from the same period, we can understand the nature of the sunward photofield. Expressing the effect of the photofield on EFW in its most general Fourier decomposition, the effect of the total field on EFW is

$$E_{\mathrm{tot}}(\theta) = E_x \cos\theta - E_y \sin\theta + \sum_{n=1}^{\infty}(a_n^{\mathrm{ph}} \cos(n\theta) + b_n^{\mathrm{ph}} \sin(n\theta)) \tag{2}$$

where E_x and E_y are the electric field compontents given by EDI and θ is the spin angle to the boom from the positive X_{GSE} axis. Figure 5 shows the Fourier decomposition of one specific spin (panel (a)), the Fourier coefficients from the
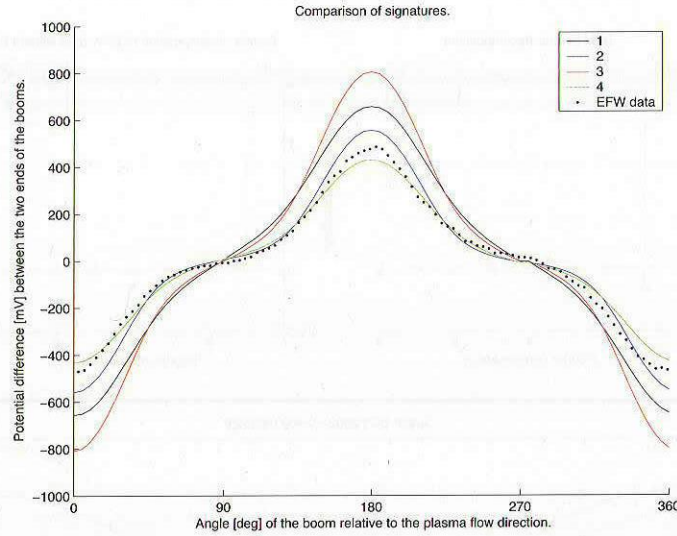
Fig. 4. Comparison of signatures from EFW data with four simulations with the spacecraft. The signatures show the potential difference between the probes at different angles of the boom relative to the flow. The EFW data is taken from the pair of probes 34 of the EFW instrument on Cluster 3 during one spin period (4 s) starting at 2002-02-13 01:48:06. In the simulations the spacecraft potential and density are constant, V=35 V and n_0=0.2 cm^{-3}, while the temperatures are varied: 1. $KT_e = KT_i = 2$ eV. 2. $KT_e = KT_i = 1$ eV. 3. $KT_e = 2$ eV, $KT_i = 1$ eV. 4. $KT_e = 1$ eV, $KT_i = 2$ eV. The amplitude of the spurious electric field varies from 4-10 mV/m.

photofield, a_n^{ph} and b_n^{ph}, (panel (b)) and the different components of the signature (panel (c)). This example together with numerous other events have shown that the photofield has the following properties:

1) The even coefficients in the Fourier expansion are negligible, as is to be expected for a differential signal.

2) The fundamental frequency is constituted almost only by $\cos\theta$ (b_1 very small, i.e. the spurious field is in the sunward-antisunward direction, as expected).

3) The odd coefficients are vanishingly small for $n > 1$.

This means that the apparent photoasymmetry signal to a very good approximation can be written as $E_{ph}(\theta) = a_1^{ph}\cos\theta = E_{ph}^0\cos\theta$.

As can clearly be seen in Figure 6.2, the photofield is dependent on the spacecraft potential. The photofield seems to increase with increasing satellite potential, but saturates at a certain value (around 1.2 mV/m). This is consistent with the model by Pedersen [11] suggesting that the photoelectron current consists of two different populations at temperatures 2 eV and 7.5 eV. When the satellite potential gets larger than $KT_{e_{ph}}/e$, all photoelectrons will be attracted by the satellite with booms regardless of the exact value of the potential. It may be noted that the value of 1.2 mV/m typical for Cluster EFW is very small compared to some earlier instruments with less degree of symmetry. For instance, the typical value on GEOS was 8 mV/m [10].

4.2 Wake field

Knowing the photoasymmetry induced field, we can also derive properties of the wake, such as direction, amplitude and shape. We now assumue that the impact on EFW on the wake field can be written as

$$E_w = a_{w1}\cos\theta_b + a_{w3}\cos(3\theta_b) + a_{w5}\cos(5\theta_b),\qquad(3)$$

where θ_b is the angle between the boom and the direction of the wake flow in the spin plane (see Figure 7), explaining that we only have contributions from cosine. In this model, we assume no time varying fields during the spin, so that by symmetry all even Fourier components are zero. We also neglect all terms higher than fifth, which should be accurate for wide wakes (such as in Figure 2). Narrow wakes occur for example in the solar wind, but do not normally constitute a large problem since they are easily detectable in EFW data.

Introducing θ_w as the angle between the positive X_{GSE} direction and the wake, the total electric field signature can be expressed as
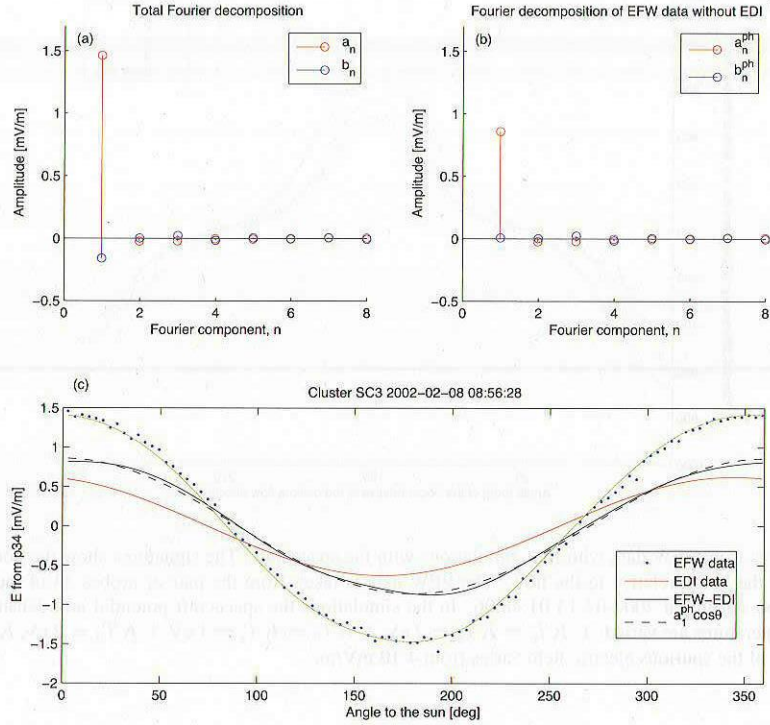
Fig. 5. Fourier decomposition of one spin from 2002-02-08 08:56:28 for probe pair 34 on spacecraft 3. Panel (a) shows the complete decomposition of the spin, while panel (b) displays the Fourier decomposition with the background electric field from EDI subtracted. In panel (c) the data (blue) is shown together with the complete Fourier decomposition (green), the EDI field (red), the resulting field from (b) (solid black) and $E_{\mathrm{ph}}^{\theta} \cos \theta$ (dashed black).
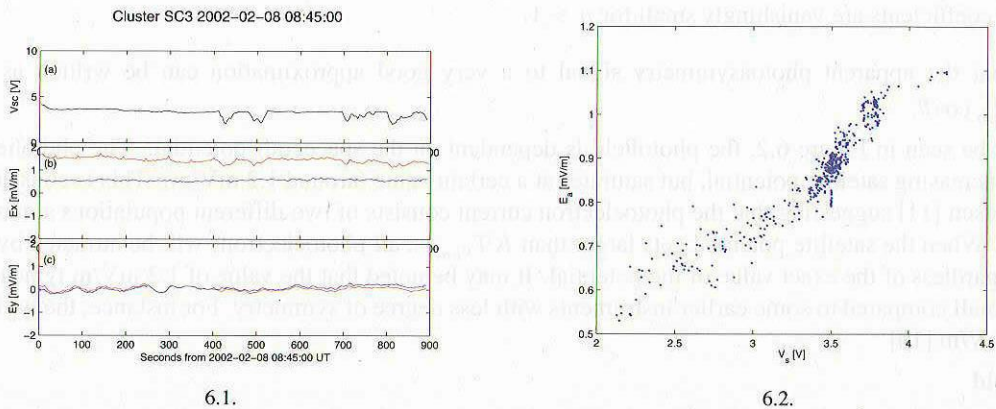

Fig. 6. 1. EFW (red) and EDI (blue) data in the satellite reference system during 920 s from 2002-02-08 08:45:00. (a) Satellite potential, V_{sc}. (b) x component of electric field data from EFW and EDI.(c) y component of electric field from EFW and EDI. 2. Dependence of the photofield on the satellite potential from the event in (1).

$$E_{\mathrm{tot}}(\theta) = (E_x + E_{\mathrm{ph}}^0 + a_{\mathrm{w}1} \cos \theta_{\mathrm{w}}) \cos \theta + (-E_y + a_{\mathrm{w}1} \sin \theta_{\mathrm{w}}) \sin \theta +$$
$$+ a_{\mathrm{w}3} \cos(3\theta_{\mathrm{w}}) \cos(3\theta) + a_{\mathrm{w}3} \sin(3\theta_{\mathrm{w}}) \sin(3\theta) + \qquad (4)$$
$$+ a_{\mathrm{w}5} \cos(5\theta_{\mathrm{w}}) \cos(5\theta) + a_{\mathrm{w}5} \sin(5\theta_{\mathrm{w}}) \sin(5\theta).$$

From a Fourier analysis of EFW spin data, we can now retrieve the direction of the wake in the spin plane, θ_{w}, the
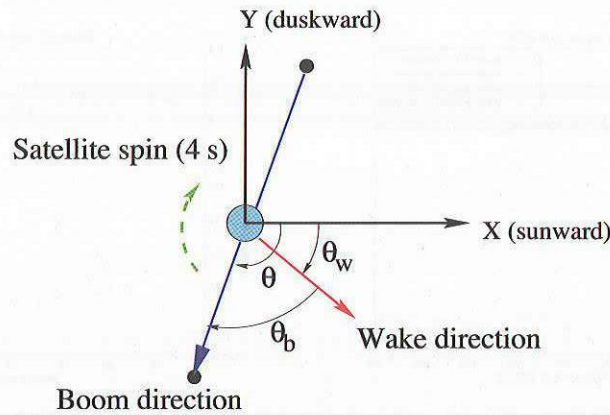
Fig. 7. Angles in the spacecraft spin plane: θ_b – angle between the boom and the direction of the wake flow, θ_w – angle between the positive X_{GSE} direction and the wake, θ – angle between the positive X_{GSE} direction and the boom.
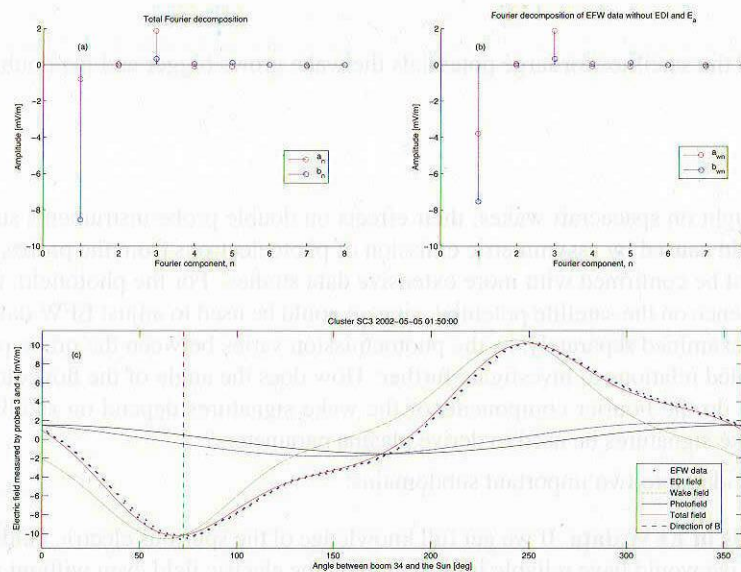

Fig. 8. Fourier decomposition of one spin for wake affected EFW data from 2002-05-05 01:50:00 for probe pair 34 on spacecraft 3. Panel (a) shows the complete decomposition of the spin, while panel (b) displays the Fourier decomposition with the background electric field from EDI and the sunward offset field subtracted. In panel (c) the data (blue) is shown together with the complete Fourier decomposition (red), the EDI field (blue), $E_{\mathrm{ph}}^0 \cos\theta$ (black), and the wake field (green).

wake Fourier components, $a_{\mathrm{w}1}$, $a_{\mathrm{w}3}$ and $a_{\mathrm{w}5}$, which describes the depth and shape of the wake, and the amplitude of the photoelectron field, E_{ph}^0. As the EFW data gives 6 Fourier components, but only 5 variables, the system of equations is overdetermined. We choose to derive θ_{w} both from the third and fifth Fourier components, since it is not uniquely determined: $\theta_{\mathrm{w}3}$ can take 6 different values ($\theta_{\mathrm{w}3} = \frac{1}{3}\arctan(b_3/a_3) + \frac{n\pi}{3}$) and $\theta_{\mathrm{w}5}$ 10 different values ($\theta_{\mathrm{w}5} = \frac{1}{5}\arctan(b_5/a_5) + \frac{n\pi}{5}$). The correct angle is found by minimizing the difference between $\theta_{\mathrm{w}3}$ and $\theta_{\mathrm{w}5}$. A small difference indicates that we have found the right angle and also confirms the validity of our model of the wake stated in equation (3). Figure 8 shows the EFW data during one spin together with the photoelectron and wake fields.

Performing the Fourier analysis for a number of subsequent spins, we can see how the wake direction changes with time (see Figure 9.1), but also investigate relations between the satellite potential and the wake field (see Figure 9.2). As can be seen in Figure 9.1, the direction of the wake in the spin plane is almost anti-parallel with the magnetic field component in the spin plane, which is expected for small perpendicular electric fields implying a plasma flow mostly along the magnetic field. Figure 9.2 gives the ratios $a_{\mathrm{w}3}/a_{\mathrm{w}1}$ and $a_{\mathrm{w}5}/a_{\mathrm{w}1}$ as a function of the satellite potential. The absolute value of both ratios tends to decrease as the satellite potential increases, which confirms the model with an enhanced wake created by
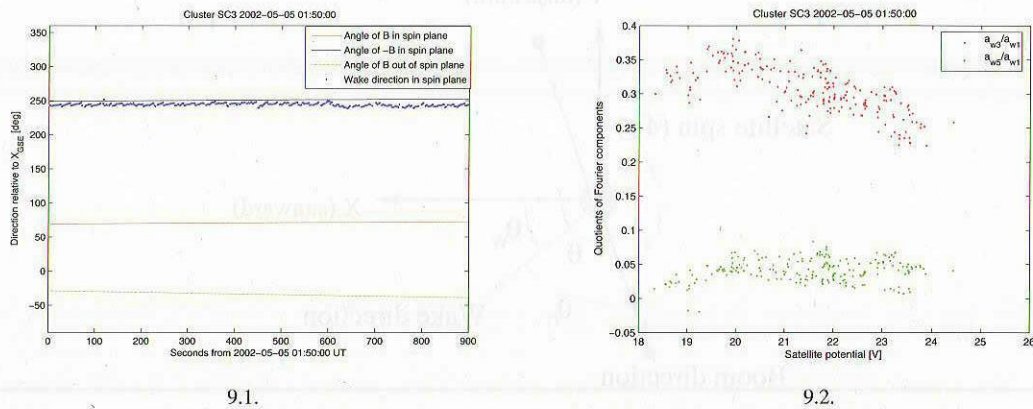
9.1.

9.2.

Fig. 9. 1. Angles versus time: Derived angles of the wake (blue), $\alpha = 360 \deg - \wedge (X_{\text{GSE}}, \mathbf{B})$ in spin plane (red), $\alpha + 180 \deg$ (black), and elevation angle of $\mathbf{B}$ out of the spin plane. 2. Dependence of the wake Fourier components on the satellite potential. Red dots corresponds to a_{w3}/a_{w1}, while green dots represents a_{w5}/a_{w1}.

potential structures around the satellite: for large potentials the wake grows bigger and the double-probe signal becomes more sinusoidal.

5. Discussion

This study has shed new light on spacecraft wakes, their effects on double probe instruments such as Cluster EFW, and in addition the sunward field caused by assymmetric emission of photoelectrons from the probes. Many of the results are still preliminary and should be confirmed with more extensive data studies. For the photofield, it would be rewarding to establish a reliable dependence on the satellite potential, since it could be used to adjust EFW data. Each probe pair on all four spacecraft should be examined separately, as the photoemission varies between the probe pairs. For the wake field, there are more yet unrevealed relations to investigate further: How does the angle of the flow out of the spin plane affect the wake signature? How do the Fourier components of the wake signatures depend on satellite potential and plasma parameters? Could the wake signatures be used to derive plasma parameters?

Future studies could be divided into two important subdomains:

Removal of spurious fields in EFW data If we get full knowledge of the spurious electric fields, they could be removed from EFW data and we would have reliable information on the electric field even without any EDI data.

Information about cold ions As described in section 3, the simulations together with data analysis from different instruments on Cluster could be used to derive properties of the wake.

6. Conclusions

The main conclusions of the current study are:

1) We have shown that the sunward photoelectron field contaminating double-probe measurements is sinusoidal: $E_{\text{ph}}(\theta) = E_{\text{ph}}^0 \cos \theta$.

2) An enhanced wake forms behind a spacecraft in a flowing plasma, when the condition $KT_i < E_k^i < eV_s$ is satisfied. Such a wake will affect a double-probe electric field instrument significantly.

3) By Fourier analysis of the disturbed EFW signal, it is possible to determine the angle, shape and size of the wake.

4) The model for the wake field, $E_w = a_{w1} \cos \theta_b + a_{w3} \cos(3\theta_b) + a_{w5} \cos(5\theta_b)$, is consistent with data.

5) Simulations with PicUp3D have given more information on the enhanced wake formation and has permitted to quantify the effect on the double-probe electric field instrument, assuming that the probes perfectly couple to the plasma. The magnitude as well as the spin dependence of the wake field is in good agreement with Cluster data. These simulations together with data analysis, could constitute a possible method to derive information about cold ions.

References

[1] Y.-J. Su, J.L. Horwitz, T.E. Moore, B.L. Giles, M.O. Chandler, P.D. Craven, M. Hirahara, and C.J. Pollock. Polar wind survey with the Thermal Ion Dynamics Experiment/Plasma Source Instrument suite aboard POLAR. *Journal of Geophysical Research*, 103:29305–29337, 1998.

[2] J.-A. Sauvaud, R. Lundin, H. Rème, J. McFadden, C. Carlson, G. Parks, E. Möbius, L. M. Kistler, B. Klecker, E. Amata, A. M. DeLellis, V. Formisano, J. M. Bosqued, I. Dandouras, P. Décréau, M. Dunlop, L. Eliasson, A. Korth, B. Lavraud, and M. McCarthy. Intermittent thermal plasma acceleration linked to sporadic motions of the magnetopause, first Cluster results. *Annales Geophysicae*, 19:1523–1532, 2001.

[3] J.-A. Sauvaud, P. Louarn, G. Fruit, H. Stenuit, C. Vallat, J. Dandouras, H. Rème, M. André, A. Balogh, M. Dunlop, L. Kistler, E. Möbius, C. Mouikis, B. Klecker, G. K. Parks, J. McFadden, C. Carlson, F. Marcucci, G. Pallocchia, R. Lundin, A. Korth, and M McCarthy. Case studies of the dynamics of ionospheric ions in the Earth's magnetotail. *Journal of Geophysical Research*, 109, doi: 10.1029/2003JA009996 2004.

[4] J. Forest, L. Eliasson, and A. Hilgers. A new spacecraft plasma simulation software, PicUp3D/SPIS. In *7th Spacecraft Charging Technology Conference*, volume SP-476, pages 515–520. ESA, 2001.

[5] G. Gustafsson et al. First results of electric field and density observations by Cluster EFW based on initial months of operation. *Annales Geophysicae*, 19:1219–1240, 2001.

[6] G. Paschmann et al. The Electron Drift Instrument on Cluster: overview of first results. *Annales Geophysicae*, 19:1273–1288, 2001.

[7] A. Eriksson, M. André, B. Klecker, H. Laakso, P.-A. Lindqvist, F. Mozer, G. Paschmann, A. Pedersen, J. Quinn, R. Torbert, K. Torkar, and H. Vaith. Cluster comparison of the double-probe and electron drift techniques for measuring the electric field. Submitted to Annales Geophysicae, June 2004.

[8] E. Engwall, A. Eriksson, A. Pedersen, J. Forest, G. Paschmann, J. Quinn, R. Torbert, and K. Torkar. Wake effects on positively charged spacecraft in flowing tenuous plasmas: Cluster observations and modeling. In *Proceedings of the 8th Spacecraft Charging Technology Conference*. NASA, 2003.

[9] E. Engwall. Numerical studies of spacecraft-plasma interaction: Simulations of wake effects on the Cluster electric field instruments EFW. IRF Scientific Report 284, Swedish Institute of Space Physics, 2004.

[10] A. Pedersen, R. Grard, K. Knott, D. Jones, A. Gonfalcone, and U. Fahleson. Measurements of quasi-static electric fields between 3 and 7 Earth radii on Geos-1. *Space Sci. Rev.*, 22:333–346, 1978.

[11] A. Pedersen. Solar wind and magnetosphere plasma diagnostics by spacecraft electrostatic potential measurements. *Annales Geophysicae*, 13:118–121, 1995.